PERGAMON

International Journal of Solids and Structures 40 (2003) 1203–1224

INTERNATIONAL JOURNAL OF SOLIDS and STRUCTURES

www.elsevier.com/locate/ijsolstr

Effects of pretwist and presetting on coupled bending vibrations of rotating thin-walled composite beams

S.-Y. Oh [a], O. Song [b], L. Librescu [a,*]

[a] *Department of Engineering Science and Mechanics, Virginia Polytechnic Institute and State University, Mail Code (0219), Blacksburg, VA 24061, USA*

[b] *Department of Mechanical Engineering, Chungnam National University, Taejon 305-764, South Korea*

Received 30 October 2001; received in revised form 10 October 2002

Abstract

A refined dynamic theory of rotating blades modeled as anisotropic composite thin-walled beams, experiencing the flapping-lagging-transverse shear coupling is presented. The structural model encompasses a number of non-standard features, such as anisotropy and transverse shear, pretwist and presetting angles, the presence of a rigid hub on which the beam is mounted, and the rotatory inertia. The developed theory and the methodology used to determine the eigenfrequency characteristics are validated against the results available in the literature, and new results emphasizing the influence played by the ply-angle, pretwist and presetting, coupled with that of the rotating speed on blade free vibration characteristics are supplied, and pertinent conclusions are outlined.

Keywords: Free vibration; Thin-walled composite beams; Presetting and pretwist; Rotating beams; Shearable beam model

1. Introduction

The accurate prediction of free vibration characteristics of turbine blades, tilt-rotor aircraft, helicopter blades and aircraft propellers is of a considerable importance towards the reliable design of these structural systems. A good knowledge of their free vibration characteristics is essential toward determination of their dynamic response to external excitations, resonant behavior, flutter instability and of their fatigue life.

In order to be able to predict adequately the free vibration response of advanced rotating blades constructed of composite materials, comprehensive structural models that encompass a number of features such as anisotropy and transverse shear warping restraint, and the pretwist and presetting angles should be developed and used. Traditionally, this problem, considered in specialized contexts, was approached within a solid isotropic beam model. In this sense, the reader is referred e.g. to the papers by Slyper (1962), Carnegie and Thomas (1972), Subrahmanyam et al. (1981), and Banerjee (2001), where, problems of

* Corresponding author. Tel.: +1-540-231-5916; fax: +1-540-231-4574.
E-mail address: librescu@vt.edu (L. Librescu).

0020-7683/02/$ - see front matter
PII: S0020-7683(02)00605-4

non-rotating beams have been addressed; to Kumar (1974), Putter and Manor (1978); Wang et al. (1926), Hodges (1981), Hodges and Rutkowski (1981), Rosen et al. (1987), where issues on vibration of rotating solid beams have been developed; and to the survey-paper by Rosen (1991) where ample references to the literature addressing various related issues have been supplied. Within the concept of thin-walled beams (TWBs), the treatment of the free vibration problem of rotating beams was carried out in various specialized contexts in a number of papers (see e.g. Rehfield et al., 1990; Chandra and Chopra, 1992; Song and Librescu, 1997, 1999; Song et al., 2001a,b; Jung et al., 2001). The survey papers, by Jung et al. (1999), Hodges (1990) and Kunz (1994) supply extensive references on the state-of-the-art of this problem.

However, in spite of the extensive work devoted to this problem, one should remark the absence of a structural model of rotating TWBs encompassing the basic features of advanced filamentary composite structural systems, such as directionality and transverse shear, as well as the pretwist and presetting effects. Within this paper, the coupled flapping-lagging-transverse shear vibrations of a pretwisted rotating composite TWB mounted on a rigid hub of radius R_0 at a setting angle γ, and featuring the previously mentioned effects are investigated.

In this context, the effects of the ply-angle of the filamentary constituent materials and of transverse shear, as well as that of the hub radius and angular velocity on coupled bending vibrations are addressed. In addition, comparisons with a number of predictions obtained in special cases are presented, and excellent agreements are reported.

2. Analysis

2.1. Preliminaries

The case of a straight pretwisted flexible beam of length L mounted on a rigid hub of radius R_0, rotating at the constant angular velocity Ω as shown in Fig. 1 is considered. The beam is allowed to vibrate flexurally in a plane making an angle γ, referred to as setting angle with the plane of rotation. The origin of the rotating systems of coordinates (x, y, z) is located at the blade root, at an offset R_0 from the rotation axis.

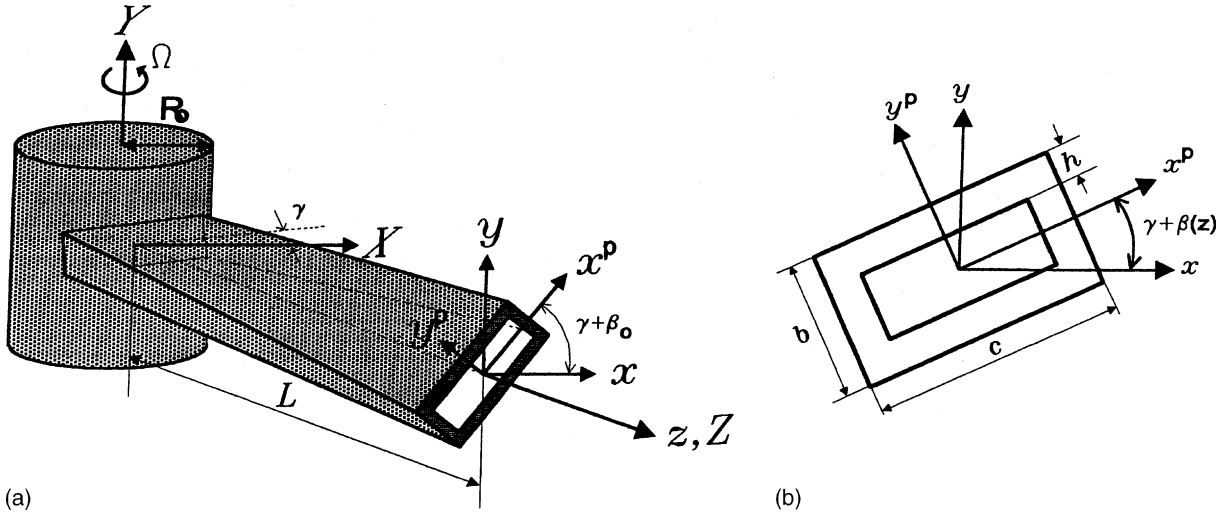

Fig. 1. (a) Geometry of the pretwisted beam. (b) Cross-section of the beam with pretwist and presetting angles.

Besides the rotating coordinates (x, y, z), we also define the local coordinates (x^p, y^p, z^p), where x^p and y^p are the *principal axes* of an arbitrary beam cross-section (see Song et al., 2001a,b).

The two coordinate systems are related by the following transformation formulae:

$$\begin{aligned} x &= x^p \cos(\gamma + \beta(z)) - y^p \sin(\gamma + \beta(z)), \\ y &= x^p \sin(\gamma + \beta(z)) + y^p \cos(\gamma + \beta(z)), \\ z &= z^p, \end{aligned} \tag{1a–c}$$

where $\beta(z) = \beta_0 z/L$ denotes the pretwist angle of a current beam cross-section, β_0 denoting the pretwist at the beam tip.

In addition to the previously defined coordinate systems, the inertial reference system (X, Y, Z) is attached to the center of the hub O. By $(\mathbf{i}, \mathbf{j}, \mathbf{k})$ and $(\mathbf{I}, \mathbf{J}, \mathbf{K})$ we define the unit vectors associated with the rotating and inertial coordinates, (x, y, z) and (X, Y, Z), respectively. In addition, a local (surface) coordinate systems (s, z, n) is considered. The geometric configuration and the typical cross-section, along with the associated systems of coordinates are presented in Fig. 1.

Within the present work, the precone angle of the blade is assumed to be zero. It is further assumed that the rotation takes place in the plane (X, Z) with the constant angular velocity $\mathbf{\Omega}(\equiv \Omega\mathbf{J} = \Omega\mathbf{j})$, the spin axis being along the Y-axis.

The considered structural model corresponds to a single-cell TWB of uniform closed-section, where the spanwise, z-coordinate axis coincides with a straight unspecified reference longitudinal axis.

2.2. Kinematics

The position vector of a point $M(x, y, z)$ belonging to the deformed beam structure is expressed as:

$$\mathbf{R}(x, y, z; t) = (x + u)\mathbf{i} + (y + v)\mathbf{j} + (z + w)\mathbf{k} + \mathbf{R}_0, \tag{2}$$

where x, y and z are the Cartesian coordinates of the points of the 3-D continuum in its undeformed state, while u, v and w denote displacement components. Recalling that the spin rate was assumed to be constant, keeping in mind that the rotation takes place solely in the XZ plane, and making use of equations expressing the time derivatives of unit vectors $(\mathbf{i}, \mathbf{j}, \mathbf{k})$, one obtain the velocity and acceleration vectors of an arbitrary point M of the beam under the form

$$\dot{\mathbf{R}} = V_x\mathbf{i} + V_y\mathbf{j} + V_z\mathbf{k} \tag{3a}$$

and

$$\ddot{\mathbf{R}} = a_x\mathbf{i} + a_y\mathbf{j} + a_x\mathbf{k} \tag{3b}$$

respectively. Their components are as follows:

$$V_x = \dot{u} + (R_0 + z + w)\Omega; \quad V_y = \dot{v}; \quad V_z = \dot{w} - (x + u)\Omega \tag{4a–c}$$

and

$$a_x = \ddot{u} + \underline{2\dot{w}\Omega} - \underline{\underline{(x + u)\Omega^2}}; \quad a_y = \ddot{v}, \quad a_z = \ddot{w} - \underline{2\dot{u}\Omega} - \underline{\underline{(R_0 + z + w)\Omega^2}}. \tag{5a–c}$$

In these equations and the following ones, the superposed dots denote time derivatives, and the terms underscored by one or two superposed solid lines are associated with Coriolis and centrifugal inertia terms, respectively. As concerns the components of the displacement vector, their expressions have been supplied by Song and Librescu (1997) and Librescu et al. (1997), and are reproduced here for completion

$$u(x,t,z;t) = u_0(z;t) - y\phi(z;t); \quad v(x,y,z;t) = v_0(z;t) + x\phi(z;t),$$
$$w(x,t,z;t) = w_0(z;t) + \theta_x(z;t)\left[y(s) - n\frac{\mathrm{d}x}{\mathrm{d}s}\right] + \theta_y(z;t)\left[x(s) + n\frac{\mathrm{d}y}{\mathrm{d}s}\right] - \phi'(z;t)[F_w(s) + na(s)]. \tag{6a–c}$$

In these equations $u_0(z;t)$, $v_0(z;t)$, $w_0(z;t)$ denote the rigid body translations along the x-, y- and z-axes, while $\phi(z;t)$ and $\theta_x(z;t)$, $\theta_y(z,t)$ denote the twist about the z-axis and rotations about the x- and y-axes respectively. The expressions of θ_x and θ_y are

$$\theta_x(z;t) = \gamma_{yz}(z;t) - v_0'(z;t); \quad \theta_y(z;t) = \gamma_{xz}(z;t) - u_0'(z;t). \tag{7a, b}$$

In Eqs. (6a–c), $F_w(s)$ and $na(s)$ play the role of primary and secondary warping functions, respectively. For their definition, see e.g. Song and Librescu (1997) and Song et al. (2001a,b).

In the absence of transverse shear effects where, γ_{xz} and γ_{yz} denote transverse shear strains,

$$\theta_x(z;t) = -v_0'(z;t); \quad \theta_y(z;t) = -u_0'(z;t). \tag{8a, b}$$

In these equations, as well as in the forthcoming ones, the primes denote differentiation with respect to the longitudinal z-coordinate.

2.3. The equations of motion and boundary conditions

In order to derive the equations of motion and the associated boundary conditions, the extended Hamilton's principle is used. This can be stated as (see e.g. Librescu, 1975)

$$\delta J = \int_{t_0}^{t_1}\left[\int_\tau \sigma_{ij}\delta\varepsilon_{ij}\,\mathrm{d}\tau - \delta K - \delta\mathscr{A} - \int_\tau \rho H_i \delta v_i\,\mathrm{d}\tau\right]\mathrm{d}t = 0, \tag{9}$$

where σ_{ij} and ε_{ij} stand for the 3-D stress and strain tensors, respectively,

$$U = \frac{1}{2}\int_\tau \sigma_{ij}\varepsilon_{ij}\,\mathrm{d}\tau \quad \text{and} \quad K = \frac{1}{2}\int_\tau \rho(\dot{\mathbf{R}}\cdot\dot{\mathbf{R}})\,\mathrm{d}\tau \tag{10a, b}$$

denote the strain energy functional and the kinetic energy, respectively.

In these equations, t_0 and t_1 denote two arbitrary instants of time; $\mathrm{d}\tau(\equiv \mathrm{d}n\,\mathrm{d}s\,\mathrm{d}z)$ denotes the differential volume element, H_i denote the components of the body forces; ρ denotes the mass density; an undertilde sign identifies a prescribed quantity, while δ denotes the variation operator. In Eqs. (9) and (10) the Einstein summation convention applies to repeated indices, where Latin indices range from 1 to 3. In the same equations, $(v_1, v_2, v_3) \equiv (u, v, w)$, and $(x_1, x_2, x_3) \equiv (x, y, z)$.

As necessary pre-requisites, the various energies that are involved in the variational principal have to be rendered explicitly.

For this case, we have:

$$\int_{t_0}^{t_1}\delta K\,\mathrm{d}t = \int_{t_0}^{t_1}\int_\tau(\dot{\mathbf{R}}\cdot\delta\dot{\mathbf{R}})\,\mathrm{d}\tau\,\mathrm{d}t = -\int_{t_0}^{t_1}\mathrm{d}t\int_\tau \rho\ddot{\mathbf{R}}\cdot\delta\mathbf{R}\,\mathrm{d}\tau, \tag{11}$$

where Hamilton's condition $\delta\mathbf{R} = 0$, for $t = t_0$, t_1 is involved.

Upon substituting (3) and (6) into (11), and performing the integrations in the circumferential and thickness directions, one obtains

$$\int_{t_0}^{t_1}\delta K\,\mathrm{d}t=\int_{t_0}^{t_1}\left\{\int_0^L-\{b_1(\ddot{u}_0+\underline{2\dot{w}_0\Omega}-\underline{\underline{u_0\Omega^2}})\delta u_0+b_1\ddot{v}_0\delta v_0+b_1[\ddot{w}_0-\underline{2\dot{u}_0\Omega}-\underline{\underline{(R_0+z+w_0)\Omega^2}}]\delta w_0$$
$$+(b_5+\delta_n b_{15})(\ddot{\theta}_y-\underset{\sim\sim\sim\sim}{\Omega^2\theta_y})\delta\theta_y+[(b_4+\delta_n b_{14})(\ddot{\theta}_x-\underset{\sim\sim\sim\sim}{\Omega^2\theta_x})+\underline{2b_4\Omega\dot{\phi}}]\delta\theta_x$$
$$+[(b_4+b_5)\ddot{\phi}-\underline{2b_4\Omega\dot{\theta}_x}-\underline{\underline{(b_4-b_5)\Omega^2}}\phi-(b_{10}+\delta_n b_{18})(\underline{\ddot{\phi}}''-\underset{===}{\Omega^2\phi''})]\delta\phi\}\,\mathrm{d}z$$
$$-[(b_{10}+\delta_n b_{18})(\underline{\ddot{\phi}}'-\underset{===}{\Omega^2\phi'})]\delta\phi]_0^L\Bigg\}\mathrm{d}t. \tag{12}$$

For the variation of the strain energy δU one obtains

$$\int_{t_0}^{t_1}\int_\tau\sigma_{ij}\delta\varepsilon_{ij}\,\mathrm{d}\tau\,\mathrm{d}t=\int_{t_0}^{t_1}\int_0^L-\{T_z'\delta w_0+(M_y'-Q_x)\delta\theta_y+(M_x'-Q_y)\delta\theta_x+[\underline{B_\omega''}+M_z'+(T_r\phi')']\delta\phi$$
$$+[Q_x'+(T_zu_0')']\delta u_0+[Q_y'+(T_zv_0')']\delta v_0\}\,\mathrm{d}z\,\mathrm{d}t+\int_{t_0}^{t_1}\big[T_z\delta w_0.+M_y\delta\theta_y+M_x\delta\theta_x$$
$$-\underline{B_\omega}\underline{\delta\phi}'+(\underline{B_\omega'}+M_z+T_r\phi')\delta\phi+(Q_x+T_zu_0')\delta u_0+(Q_y+T_zv_0')\delta v_0\big]_0^L\,\mathrm{d}t. \tag{13}$$

These equations are represented in terms of 1-D stress resultants (T_z, Q_x and Q_y) and stress couples (M_x, M_y, M_z, T_r and B_w). Their expressions have been supplied by Song and Librescu (1993), and will not be recorded here.

Considering also the virtual work of external forces we have,

$$\delta\mathscr{A}=\int_0^L[p_x\delta u_0+p_y\delta v_0+p_z\delta w_0+m_x\delta\theta_x+m_y\delta\theta_y+(m_z+m_\omega')\delta\phi]\,\mathrm{d}z$$
$$+\left[\underset{\sim}{Q}_x\delta u_0+\underset{\sim}{Q}_y\delta v_0+\underset{\sim}{T}_z\delta w_0+\underset{\sim}{M}_x\delta\theta_x+\underset{\sim}{M}_y\delta\theta_y+\underset{\sim}{M}_z\delta\phi-\underset{\sim}{B}_\omega\delta\phi'\right]\Big|_0^L. \tag{14}$$

Using (12)–(14) in the Hamilton's principle, invoking the stationarity of the functional in the time internal $[t_0,t_1]$ and the fact that the variations (δu_0, δv_0, δw_0, $\delta\theta_x$, $\delta\theta_y$, $\delta\phi$ and $\delta\phi'$) are independent and arbitrary, their coefficients in the two integrand must vanish independently. This yields the equations of motion and the boundary condition, that are not displayed here.

3. Governing system

3.1. The shearable system

In the present paper a special case of ply-angle distribution inducing special elastic couplings will be considered. This consists of the lamination scheme

$$\theta(x)=\theta(-x),\quad \theta(y)=\theta(-y), \tag{15}$$

where θ denotes the ply-angle orientation considered to be positive when is measured from the positive s-axis towards the positive z-axis (see Fig. 1).

As it was previously shown, (see Atilgan and Rehfield, 1989; Smith and Chopra, 1991), this ply-angle configuration, referred to as the *circumferentially uniform stiffness* configuration achievable via the usual filament winding technology, results in an exact decoupling between flapping-lagging-transverse shear, on one hand, and extension-torsional motion, on the other hand. In the present study only the former problem involving the bending–bending coupling will be considered.

The governing dynamical equations of pretwisted rotating blades expressed in terms of displacement variables are expressed as:

$$
\begin{aligned}
&\delta u_0 : \Big[a_{42}(z)\theta_y' + a_{43}(z)\theta_x' + a_{44}(z)(u_0' + \theta_y) + a_{45}(z)(v_0' + \theta_x)\Big]' - b_1\ddot{u}_0 + \underline{\underline{b_1 u_0 \Omega^2}} \\
&\quad + \underline{\underline{b_1 \Omega^2 [R(z)u_0']'}} + p_x = 0, \\
&\delta v_0 : \Big[a_{52}(z)\theta_y' + a_{53}(z)\theta_x' + a_{55}(z)(v_0' + \theta_x) + a_{54}(z)(u_0' + \theta_y)\Big]' - b_1\ddot{v}_0 + \underline{\underline{b_1 \Omega^2 [R(z)v_0']'}} + p_y = 0, \\
&\delta\theta_y : \Big[a_{22}(z)\theta_y' + a_{25}(z)(v_0' + \theta_x) + a_{24}(z)(u_0' + \theta_y) + a_{23}(z)\theta_x'\Big]' - a_{44}(z)(u_0' + \theta_y) - a_{43}(z)\theta_x' \\
&\quad - a_{45}(z)(v_0' + \theta_x) - a_{42}(z)\theta_y' - (b_5(z) + \delta_n b_{15}(z))(\ddot{\theta}_y - \underset{\sim\sim\sim}{\Omega^2\theta_y}) \\
&\quad - (b_6(z) - \delta_n b_{13}(z))(\ddot{\theta}_x - \underset{\sim\sim\sim}{\Omega^2\theta_x}) + m_y = 0, \\
&\delta\theta_x : \Big[a_{33}(z)\theta_x' + a_{32}(z)\theta_y' + a_{34}(z)(u_0' + \theta_y) + a_{35}(z)(u_0' + \theta_x)\Big]' - a_{55}(z)(v_0' + \theta_x) - a_{52}(z)\theta_y' \\
&\quad - a_{54}(z)(u_0' + \theta_y) - a_{53}(z)\theta_x' - (b_4(z) + \delta_n b_{14}(z))(\ddot{\theta}_x - \underset{\sim\sim\sim}{\Omega^2\theta_x}) \\
&\quad - (b_6(z) - \delta_n b_{13}(z))(\ddot{\theta}_y - \underset{\sim\sim\sim}{\Omega^2\theta_y}) + m_x = 0.
\end{aligned}
\tag{16}
$$

Herein, p_x, p_y, m_x and m_y are the external loads and moments that are assumed to be functions of both z and t coordinates.

For the sake of identification, in the previous equations, the terms associated with the centrifugal acceleration terms are underscored by two superposed solid lines (====); rotatory inertia terms by a dotted line $(\cdots)$, and centrifugal-rotatory effect by a solid line superposed on a wavy line ($\underset{\sim\sim\sim}{}$).

Assuming the blade to be clamped at $z = 0$ and free at $z = L$, the homogeneous boundary conditions result as:

At $z = 0$:

$$
u_0 = 0, \quad v_0 = 0, \quad \theta_x = 0, \quad \theta_y = 0 \tag{17}
$$

and at $z = L$:

$$
\begin{aligned}
&\delta u_0 : a_{42}(L)\theta_y' + a_{43}(L)\theta_x' + a_{44}(L)(u_0' + \theta_y) + a_{45}(L)(v_0' + \theta_x) = 0, \\
&\delta v_0 : a_{52}(L)\theta_y' + a_{53}(L)\theta_x' + a_{55}(L)(v_0' + \theta_x) + a_{54}(L)(u_0' + \theta_y) = 0, \\
&\delta\theta_y : a_{22}(L)\theta_y' + a_{25}(L)(v_0' + \theta_x) + a_{24}(L)(u_0' + \theta_y) + a_{23}(L)\theta_x' = 0, \\
&\delta\theta_x : a_{33}(L)\theta_x' + a_{34}(L)(u_0' + \theta_y) + a_{35}(L)(v_0' + \theta_x) + a_{32}(L)\theta_y' = 0.
\end{aligned}
\tag{18}
$$

As is clearly seen, these equations can address either the dynamic response of rotating blades exposed to time-dependent external excitation, or the free vibration problem. In the latter case, the external loads should be discarded.

In Eq. (16) and the following ones

$$
R(z) \equiv \left[R_0(L - z) + \tfrac{1}{2}(L^2 - z^2)\right], \tag{19}
$$

whereas the coefficients $a_{ij}(z) = a_{ji}(z)$ and $b_i(z)$ denote stiffness and reduced mass terms, respectively. Their expressions are displayed in Tables 1 and 2, respectively.

Table 1
Expressions of stiffness quantities ($a_{ij}(z) = a_{ji}(z)$), in terms of their cross-sectional principal axes x^p and y^p counterparts, $a^p_{ij}(= a^p_{ji})$, pretwist and presetting angles

$a_{ij}(z)$	Their expression
a_{22}	$a^p_{22}\cos^2(\gamma+\beta(z)) + a^p_{33}\sin^2(\gamma+\beta(z)) - 2a^p_{23}\sin(\gamma+\beta(z))\cos(\gamma+\beta(z))$
a_{33}	$a^p_{33}\cos^2(\gamma+\beta(z)) + a^p_{22}\sin^2(\gamma+\beta(z)) + 2a^p_{23}\sin(\gamma+\beta(z))\cos(\gamma+\beta(z))$
a_{44}	$a^p_{44}\cos^2(\gamma+\beta(z)) + a^p_{55}\sin^2(\gamma+\beta(z)) - 2a^p_{45}\sin(\gamma+\beta(z))\cos(\gamma+\beta(z))$
a_{55}	$a^p_{55}\cos^2(\gamma+\beta(z)) + a^p_{44}\sin^2(\gamma+\beta(z)) + 2a^p_{54}\sin(\gamma+\beta(z))\cos(\gamma+\beta(z))$
a_{23}	$(a^p_{22} - a^p_{33})\sin(\gamma+\beta(z))\cos(\gamma+\beta(z))$
$a_{24} = -a_{35}$	$-(a^p_{25} + a^p_{34})\sin(\gamma+\beta(z))\cos(\gamma+\beta(z))$
a_{25}	$a^p_{25}\cos^2(\gamma+\beta(z)) - a^p_{34}\sin^2(\gamma+\beta(z)) + (a^p_{24} - a^p_{35})\cos(\gamma+\beta(z))\sin(\gamma+\beta(z))$
a_{34}	$a^p_{34}\cos^2(\gamma+\beta(z)) - a^p_{25}\sin^2(\gamma+\beta(z)) + (a^p_{24} - a^p_{35})\cos(\gamma+\beta(z))\sin(\gamma+\beta(z))$
a_{45}	$(a^p_{44} - a^p_{55})\cos(\gamma+\beta(z))\sin(\gamma+\beta(z))$

Table 2
The reduced mass terms $b_i(z)$ in terms of their counterparts in the cross-sectional principal axes b^p_i

$b_i(z)$	Their expression
b_1	b^p_1
b_4	$b^p_4\cos^2(\gamma+\beta(z)) + b^p_5\sin^2(\gamma+\beta(z)) + 2b^p_6\sin(\gamma+\beta(z))\cos(\gamma+\beta(z))$
b_5	$b^p_5\cos^2(\gamma+\beta(z)) + b^p_4\sin^2(\gamma+\beta(z)) - 2b^p_6\sin(\gamma+\beta(z))\cos(\gamma+\beta(z))$
b_6	$(b^p_5 - b^p_4)\cos(\gamma+\beta(z))\sin(\gamma+\beta(z)) + b^p_6(\cos^2(\gamma+\beta(z))) - \sin^2(\gamma+\beta(z))$
b_{13}	$(b^p_{14} - b^p_{15})\cos(\gamma+\beta(z))\sin(\gamma+\beta(z))$
b_{14}	$b^p_{14}\cos^2(\gamma+\beta(z)) + b^p_{15}\sin^2(\gamma+\beta(z)) - 2b^p_{13}\sin(\gamma+\beta(z))\cos(\gamma+\beta(z))$
b_{15}	$b^p_{15}\cos^2(\gamma+\beta(z)) + b^p_{14}\sin^2(\gamma+\beta(z)) + 2b^p_{13}\sin(\gamma+\beta(z))\cos(\gamma+\beta(z))$

The quantities affected by superscript p, indicate their affiliation to the beam cross-sections referred to the principal axes (x^p, y^p). These quantities can be found in the paper by Song and Librescu (1993).

3.2. Non-shearable counterpart of the previously obtained system

Extracting from Eqs. $(16)_3$ and $(16)_4$, the expressions $a_{44}(u_0' + \theta_y) + a_{45}(v_0' + \theta_x)$ and $a_{55}(v_0' + \theta_x) + a_{54}(u_0' + \theta_y)$, respectively, and their corresponding replacement in Eqs. $(16)_1$, $(16)_2$, $(18)_1$, and $(18)_2$ followed by consideration of $\theta_x \to -v_0'$ and $\theta_y = -u_0'$, yields the Bernoulli–Euler counterpart of the shearable beam model.

As a result, the governing equations read as:

$$\begin{aligned}
&\delta u_0 : [a_{22}(z)u_0'' + a_{23}(z)v_0'']'' - [(b_5(z) + \delta_n b_{15}(z))(\dddot{u}_0' - \underbrace{\Omega^2 u_0'}_{\sim\sim\sim\sim}) + (b_6(z) - \delta_n b_{13}(z))(\dddot{v}_0' - \underbrace{\Omega^2 v_0'}_{\sim\sim\sim\sim})']' \\
&\quad + b_1\ddot{u}_0 - \underline{b_1\Omega^2 u_0} - \underline{\underline{b_1\Omega^2[R(z)u_0']'}} - p_x - m_y' = 0, \\
&\delta v_0 : [a_{33}(z)v_0'' + a_{32}(z)u_0'']'' - [(b_4(z) + \delta_n b_{14}(z))(\dddot{v}_0' - \underbrace{\Omega^2 v_0'}_{\sim\sim\sim\sim}) + (b_6(z) - \delta_n b_{13}(z))(\dddot{u}_0' - \underbrace{\Omega^2 u_0'}_{\sim\sim\sim\sim})]' \\
&\quad + b_1\ddot{v}_0 - \underline{\underline{b_1\Omega^2[R(z)v_0']'}} - p_y - m_x' = 0.
\end{aligned} \tag{20}$$

The associated homogeneous boundary conditions are:

At $z = 0$:

$$u_0 = v_0 = u_0' = v_0' = 0 \tag{21}$$

and at $z = L$:

$$\begin{aligned}
&\delta u_0 : [a_{22}(L)u_0'' + a_{23}(L)v_0'']' - (b_5(L) + \delta_n b_{15}(L))(\ddot{\underset{\cdots}{u}}_0' - \underset{\sim\sim\sim\sim}{\Omega^2 u_0'}) \\
&\qquad - (b_6(L) - \delta_n b_{13}(L))(\ddot{\underset{\cdots}{v}}_0' - \underset{\sim\sim\sim\sim}{\Omega^2 v_0'}) - m_y(L,t) = 0, \\
&\delta v_0 : [a_{33}(L)v_0'' + a_{32}(L)u_0'']' - (b_4(L) + \delta_n b_{14}(L))(\ddot{\underset{\cdots}{v}}_0' - \underset{\sim\sim\sim\sim}{\Omega^2 v_0'}) \\
&\qquad - (b_6(L) - \delta_n b_{13}(L))(\ddot{\underset{\cdots}{u}}_0' - \underset{\sim\sim\sim\sim}{\Omega^2 u_0'}) - m_x(L,t) = 0, \\
&\delta u_0' : a_{22}(L)u_0'' + a_{23}(L)v_0'' = 0, \\
&\delta v_0' : a_{33}(L)v_0'' + a_{32}(L)u_0'' = 0.
\end{aligned} \tag{22}$$

The expressions of stiffness $a_{ij}(z)$ and reduced mass terms $b_i(z)$ are supplied in Tables 1 and 2.

4. Several comments on the governing system

In connection with the governing equations of pretwisted rotating beams several comments are in order.

First of all, it should be reminded that in the context of the implemented ply-angle configuration, the governing system, Eqs. (16)–(18), involve the flapping-lagging-transverse shear elastic couplings.

However, in the presence of the pretwist and presetting a supplementary coupling between the flapping-lagging-transverse shear motions is experienced. In this case, as emerging from Tables 1 and 2, the stiffness quantities and reduced mass terms become a function of the spanwise coordinate. It also becomes evident that for the non-pretwisted beams featuring also zero presetting, the stiffness quantities $a_{23}(z)$, $a_{24}(z)$, $a_{35}(z)$ and $a_{45}(z)$, and the mass term $b_6(z)$ (when also the rotatory inertia effect is discarded), as well as $b_{13}(z)$ become zero valued quantities, and, as a result, a number of couplings become immaterial.

Moreover, for non-pretwisted beams, the stiffness and mass terms cease to experience the spanwise dependence. It also clearly emerges that for doubly symmetric beams of a square cross-section, the stiffnesses $a_{23}(z)$, $a_{24}(z)$, $a_{35}(z)$ and $a_{45}(z)$, as well as the mass terms $b_6(z)$ and $b_{13}(z)$ become zero valued quantities for any value of the pretwist and presetting angles.

Most similar comments related to the stiffness $a_{23}(z)(= a_{32}(z))$ and mass terms $b_6(z)$ and $b_{13}(z)$ are applicable to the classical beam counterpart, as well.

We should however remark that for doubly symmetrical beam cross-sections, implying $a_{22}^p = a_{33}^p$; $b_4^p = b_5^p$ and $b_{14}^p = b_{15}^p$, and in the absence of rotatory inertia (implying $b_6^p = 0$), the two classical bending equations and the associated boundary conditions exactly decouple into two independent groups, each of these governing, for any pretwist or presetting angle, the out-of-plane and the in-plane bending. Consequently, in this special case, it results that

$$a_{22} = a_{33} \equiv S; \quad b_4(z) = b_5(z) \text{ and } b_{15}(z) = b_{14}(z). \tag{23a}$$

From the system of governing equations (20)–(22), specialized to the case of zero pretwist, one can express u_0 and v_0 as

$$[u_0(z,t); v_0(z,t)] = W(z)[\sin\gamma, \cos\gamma]\exp(\mathrm{i}\omega t), \quad [\mathrm{i} = \sqrt{-1}], \tag{23b}$$

where $W(z)$ is the deflection in the plane defined by the setting angle γ.

Expressing in (20)–(22) u and v through W, one can recast the dynamic equations governing the bending of a Bernoulli–Euler rotating beam featuring doubly symmetry, in a plane at angle γ with the plane of rotation as:

$$[SW'']'' + \{[b_5 + \delta_n b_{15}](\omega^2 + \Omega^2)W'\}' - b_1\Omega^2[R(z)W']' - b_1\omega_1^2 W = 0, \tag{24a}$$

where

$$\omega_1^2 = \omega^2 + \Omega^2 \sin^2\gamma \tag{24b}$$

and the boundary conditions:

$$W = W' = 0 \quad \text{at } z = 0 \tag{25}$$

and

$$[SW'']' + [b_5 + \delta_n b_{15}](\omega^2 + \Omega^2)W' = 0, \quad SW'' = 0, \quad \text{at } z = L. \tag{26}$$

These equations specialized for the case of the absence of rotatory inertia, reduce to those supplied by Hodges (1981).

It should be noticed that for $\gamma = \pi/2$ and 0, Eqs. (24)–(26) reduce to the rotating beam counterpart experiencing the motion in lagging and flapping, respectively.

From Eq. (24b) one can see that the flapping frequency is $\omega_1^2 \Rightarrow \tilde{\omega}^2$, while the vibration frequencies at any γ expressed in terms of that at $\gamma = 0$ can be expressed as

$$\omega^2 = \tilde{\omega}^2 - \Omega^2 \sin^2\gamma. \tag{27}$$

This expression reveals that the frequencies at any setting angle are lower than those corresponding to the purely flapping motion counterpart.

Applying the Rayleigh-quotient procedure to the governing Eq. (24) considered in conjunction with the boundary conditions and Eq. (19), the natural frequency at any setting angle results as

$$\omega^2 = \frac{\int_0^L \left\{ S(W'')^2 + \Omega^2 \left[b_1 R(z)(W')^2 - \underset{\sim\sim\sim\sim\sim\sim\sim\sim}{(b_5 + \delta_n b_{15})}(W')^2 - b_1 W^2 \sin^2\gamma \right] \right\} \mathrm{d}z}{\int_0^L \left\{ \underset{\cdots\cdots\cdots\cdots}{(b_5) + \delta_n b_{15}}(W')^2 + b_1 W^2 \right\} \mathrm{d}z}, \tag{28}$$

where $W = W(z)$ should fulfil boundary conditions, Eqs. (25) and (26).

From this equation one can easily conclude that rotatory inertia yield a diminution of fundamental frequency, whereas the increase of the rotor hub radius results in frequency increase. As concerns the setting angle, its increase yields a decrease of the fundamental frequency. These conclusions are in excellent agreement with those outlined by Lo and Renbarger (1952). The results also reveal that for the non-rotating blade, the effects of the hub radius and presetting angle on eigenfrequency are immaterial.

5. Solution procedure

Due to the intricacy of the eigenvalue problem, and of the complex character of dynamic boundary conditions, an approximate solution procedure should be applied. To this end, u_0, v_0, θ_x and θ_y are represented by means of series of space-dependent trial functions that should fulfil the boundary conditions, multiplied by time-dependent generalized coordinates.

For the problem at hand the displacement measures are represented as

$$(u_0(z,t), v_0(z,t), \theta_x(z,t), \theta_y(z,t)) = (V(z), V(z), S(z), P(z)) \exp(\mathrm{i}\omega t) \tag{29}$$

where ω is the eigenfrequency, while the spatial parts are expressed as

$$(U(z), V(z), S(z), P(z)) = \sum_{j=1}^{n} (a_j u_j(z), b_j v_j(z), c_j s_j(z), d_j p_j(z)) \tag{30}$$

In Eq. (30), $u_j(z), v_j(z), s_j(z)$ and $p_j(z)$ are the trial functions that should fulfil all the boundary conditions. However, trial functions satisfying also the dynamic boundary conditions, can hardly be generated.

In the spirit of the Extended Galerkin Method (see e.g. Librescu et al. (1997)), only admissible functions, (i.e. trial functions fulfilling only the geometrical boundary conditions), are used. As a result, the trial functions are expressed as polynomials of various power in the z variable which exactly fulfil the boundary conditions at $z = 0$.

To be consistent with the *EGM*, representations (29) in conjunction with (30) are inserted in the Hamilton's principle. Because from the boundary conditions only the dynamic boundary conditions are not fulfilled, these remain in the functional as residual terms that, together with the one resulting from the equations of motion, are minimized in the Galerkin' sense. (see e.g. Librescu et al. (1997)).

As it was previously revealed in different contexts (see e.g. Librescu et al. (1997) and Qin and Librescu (2002)), the application of this method results in an excellent accuracy and rapid convergence. For the problem at hand, the eigenvalue problem results in the standard form $\mathbf{Ax} = \omega^2\mathbf{x}$, where $\mathbf{A} = \mathbf{M}^{-1}\mathbf{K}$, $\mathbf{M}$ and $\mathbf{K}$ being the mass and stiffness $4n \times 4n$ matrices,

$$\mathbf{x}^{\mathbf{T}} = [a_1, a_2, \ldots, a_n, b_1, b_2, \ldots, b_n, c_1, c_2, \ldots, c_n, d_1, d_2, \ldots, d_n]$$

is a constant vector, while ω is the eigenfrequency.

6. Comparisons with available numerical predictions

For the case of the nonrotating thin-walled beams, extensive validations of the statics and dynamics of composite single-cell box beams have been accomplished and reported in the papers by Qin and Librescu (2001, 2002). The validations have revealed that the present thin-walled beam model provides results is excellent agreement with those based on various structural models. Among these, for static validation, there are the ones developed by Hodges and his collaborators (see e.g. Volovoi et al. (2001), as well as the ones supplied by Smith and Chopra (1991) and Rehfield et al. (1990).

For dynamic validation, the results obtained within the present model and compared with the ones by Chandra and Chopra (1992), reveal also excellent agreements. Moreover, very good agreements between the static (Smith and Chopra (1991)) and dynamic (Chandra and Chopra (1992) and their counterparts based on the present structural model, have been reported by Qin and Librescu (2001, 2002)).

The equations derived for the case of rotating TWB are similar to the ones corresponding to a *solid beam* model. The difference occurs only in the *proper* expression of cross-sectional stiffness quantities and mass terms. For this reason, use of dimensionless parameters in which these quantities are absorbed, enables one to obtain universal results, valid for both solid and TWBs. In order to validate both the solution methodology and the structural model developed in this paper, comparisons with a number of results available in the literature are presented.

In Tables 3–5, within the assumptions considered in Section 4 above, comparisons with a number of previously obtained results are displayed.

In this sense, in Table 3, the effect of the setting angle and of selected rotational speeds on the first four natural frequencies of shearable beams, is compared to that obtained in the papers by Wang et al. (1976), Yokoyama (1988), and Lee and Lin (1996), where various methods have been applied.

In these numerical simulations the following dimensionless parameters of the rotational speed, natural frequency, and hub radius have been used and are listed in the same sequence:

$$(\bar{\Omega}^2, \bar{\omega}^2) = (\Omega^2, \omega^2)(b_1 L^4/a_{33}); \quad \bar{R}_0 = R_0/L. \tag{31}$$

The results reveal the excellent agreement, especially with the predictions by Yokoyama (1988) obtained via FEM.

Table 3
Comparison of coupled flapping-lagging frequencies ω_i (Hz) of a pretwisted beam ($\beta_0 = 45$ deg., $\gamma = 0$, $\Omega = 0$, $R_0 = 0$)

ω_i	Subrahmanyam et al. (1981)		Dawson (1968) (Rayleigh–Ritz process)	Rao (1977) (Galerkin process)	Carnegie (1959) (experiment)	Present (extended Galerkin method)	Error w.r.t. experiment(%)
	Reissner method	Potential energy method					
$i = 1$	61.9	62.0	62.0	61.9	59.0	62.0	5.25
$i = 2$	304.7	305.1	301.0	305.0	290.0	305.1	5.21
$i = 3$	937.0	955.1	953.0	949.0	920.0	949.0	3.15
$i = 4$	1205.1	1214.7	1230.0	1220.0	1110.0	1206.1	8.66

The characteristics of the beam as involved in the considered table are: $a^p_{22}(\equiv EI_{yy}) = 487.9$ N m^2; $a^p_{33}(\equiv EI_{xx}) = 2.26$ N m^2, $a^p_{44} = a^p_{55}(\equiv kGA) = 3.076 \times 10^6$ N m^2, $b^p_1(\equiv \rho A_0) = 0.3447$ kg/m; $b^p_4 \equiv (\rho I_{xx}) = 8.57 \times 10^{-8}$ kg m, $b^p_5 \equiv (\rho I_{yy}) = 0.000019$ kg m, $b^p_{14} = b^0_{15} = 0$, $L = 15.24 \times 10^{-2}$ m.

Table 4
Effect of setting angle on natural frequency parameter $\bar{\omega}_i$ of rotating cantilever shearable beams ($\bar{\Omega} = 10$ and $\bar{R}_0 = 3$)

$\bar{\omega}_i$		$\eta = 0.1$, $\mu = 0.030588$			$\eta = 0.025$, $\mu = 0.007647$		
		$\gamma = 0$ deg.	$\gamma = 45$ deg.	$\gamma = 90$ deg.	$\gamma = 0$ deg.	$\gamma = 45$ deg.	$\gamma = 90$ deg.
$i = 1$	Present	23.0362	21.973	20.853	23.510	22.431	21.298
	[a]	23.050	21.987	20.867	23.524	22.446	21.313
	[b]	23.037	21.974	20.850	23.514	22.436	21.302
	[c]	22.938	21.873	20.753	23.491	22.411	21.277
$i = 2$	Present	45.429	45.195	44.957	56.062	55.653	55.240
	[a]	45.598	45.359	45.115	56.105	55.696	55.284
	[b]	45.428	45.194	44.955	56.072	55.662	55.250
	[c]	44.781	44.550	44.315	55.984	55.575	55.162
$i = 3$	Present	66.866	66.775	66.681	97.002	96.782	96.562
	[a]	67.716	67.619	67.520	97.188	96.968	96.747
	[b]	66.854	66.793	66.668	97.011	96.792	96.570
	[c]	66.287	66.200	66.109	96.913	96.693	96.473
$i = 4$	Present	72.315	72.148	71.985	144.194	144.052	143.911
	[a]	73.076	72.914	72.756	144.490	144.349	144.208
	[b]	72.313	72.146	71.982	143.815	143.673	143.531
	[c]	71.967	71.792	71.620	143.71	143.57	143.43

$\eta \equiv (b_4 + \delta_n b_{14})/(b_1 L^2)$, $\mu \equiv a_{33}/(L^2 a_{55})$.
[a] Wang et al. (1976).
[b] Yokoyama (1988).
[c] Lee and Lin (1996).

The trend of variation of natural bending frequencies with the setting angle is consistent with that emerging from Eq. (28), in the sense that the increase of γ yields a decrease of bending natural frequencies, this being valid for any mode number.

In Tables 4 and 5, within the assumptions displayed in Section 4, and for zero pretwisted rotating beams, there are displayed comparisons of flapping ($\gamma = 0$) and lagging ($\gamma = 90$ deg.) frequencies, respectively with some available results from the literature.

For $\gamma = 0$ and 90 deg., the results are compared with those supplied by Hodges and Rutkowski (1981), and Yokoyama (1988) and Putter and Manor (1978), respectively, and excellent agreements are remarked.

In Tables 6 and 7 comparisons of frequency predictions obtained for non-rotating/rotating unshearable blades including effects of pretwist and presetting angles are supplied. The analyzed beam is characterized by (see Rosen et al., 1987):

Table 5
Natural frequency parameter $\bar{\omega}_i$ of rotating unshearable cantilever beam ($\gamma = 0$, $\beta_0 = 0$)

$\bar{\Omega}$	$\bar{\omega}_1$				$\bar{\omega}_2$				$\bar{\omega}_3$			
	$\bar{R} = 0$		$\bar{R}_0 = 1$		$\bar{R}_0 = 0$		$\bar{R}_0 = 1$		$\bar{R}_0 = 0$		$\bar{R}_0 = 1$	
	Hodges and Rutkowski (1981)	Present	Hodges and Rutkowski (1981)	Present	Hodges and Rutkowski (1981)	Present	Hodges and Rutkowski (1981)	Present	Hodges and Rutkowski (1981)	Present	Hodges and Rutkowski (1981)	Present
0	3.51602	3.51602	3.51602	3.51602	22.0345	22.0344	22.0345	22.0344	61.6972	61.7150	61.6972	61.7150
1	3.68165	3.68164	3.88882	3.88882	22.1810	22.1810	22.3750	22.3750	61.8418	61.8593	62.0431	62.0607
2	4.13732	4.13732	4.83369	4.83367	22.6149	22.6149	23.3660	23.3661	62.2732	62.6149	63.0676	63.0644
3	4.79728	4.79727	6.08175	6.08173	23.3203	23.3203	24.9278	24.9278	62.9850	63.0013	64.7338	64.7493
4	5.58500	5.58500	7.47505	7.47505	24.2734	24.2734	26.9573	26.9573	63.9668	63.9820	66.9868	67.0006
5	6.44955	6.44953	8.94036	8.94042	25.4461	25.4461	29.3528	29.3528	65.2050	65.2189	69.7607	69.7725
6	7.36037	7.36038	10.4439	10.4438	26.8091	26.8091	32.0272	32.0273	66.6839	66.6963	72.9863	72.9960
7	8.29964	8.29960	11.9691	11.9690	28.3341	28.3341	34.9116	34.9117	68.3860	68.3968	76.5965	76.6039
8	9.25684	9.25683	13.5074	13.5077	29.9954	29.9954	37.9538	37.9539	70.2930	70.3022	80.5295	80.5352
9	10.2257	10.2257	15.0541	15.0542	31.7705	31.7705	41.1154	41.1161	72.3867	72.3944	84.7315	84.7352
10	11.2023	11.2025	16.6064	16.6062	33.6404	33.6403	44.3682	44.3698	74.6493	74.6556	89.1563	89.1583
11	12.1843	12.1843	18.1626	18.1628	35.5890	35.5890	47.6916	47.6941	77.0638	77.0687	93.7654	93.7667
12	13.1702	13.1702	19.7215	19.7223	37.6031	37.6033	51.0701	51.0741	79.6145	79.6181	98.5268	98.5277

Table 6
Natural frequency parameter $\bar{\omega}_i$ of rotating unshearable cantilever beams ($\gamma = 90$ deg., $\beta_0 = 0$)

$\bar{\Omega}$	$\bar{\omega}_1$						$\bar{\omega}_2$					
	$\bar{R}_0 = 0$			$\bar{R}_0 = 1$			$\bar{R}_0 = 0$			$\bar{R}_0 = 1$		
	Yokoyama (1988)	Putter and Manor (1978)	Present	Yokoyama (1988)	Putter and Manor (1978)	Present	Yokoyama (1988)	Putter and Manor (1978)	Present	Yokoyama (1988)	Putter and Manor (1978)	Present
0	3.516	–	3.51602	3.516	–	3.51602	22.036	–	22.0344	22.036	–	22.0344
2	3.622	3.6118	3.62179	4.401	4.4005	4.40054	22.528	22.5263	22.5263	23.282	23.2803	23.2802
5	4.074	4.0739	4.07390	7.412	7.4115	7.41130	24.952	24.9500	24.9500	28.926	28.9238	28.9240
10	5.050	5.0490	5.04889	13.261	13.2580	13.2576	32.123	32.1197	32.1198	43.237	43.2267	43.2282
20	6.794	6.7757	6.77927	25.318	25.2881	25.2992	51.372	51.3531	51.3573	76.659	76.5942	76.6353
50	10.899	10.4806	10.7630	61.881	61.6408	61.8446	116.417	116.1996	116.359	182.386	181.9361	182.316

$$a_{22} = 2869.7\ \mathrm{N\,m^2}; \quad a_{33} = 57,393\ \mathrm{N\,m^2}; \quad b_1 = 34.47\ \mathrm{kg/m}, \text{ and } L = 3.048\ \mathrm{m}.$$

The results obtained within the present model and solution methodology (based on the extended Galerkin method—see e.g. Librescu et al. (1997)), displayed in Tables 7 and 8 reveal a very good agreement with the available exact and approximate predictions by Rosen et al. (1987) and Banerjee (2001). Moreover, Table 8, reveals that for blades featuring $a_{22} \neq a_{33}$, and in contrast to the case considered in Table 3, for which $a_{22} = a_{33}$, $b_4 = b_5$, the increase of the setting angle yields, depending on the odd or even mode number, either a decrease or increase of natural frequencies, respectively. At the same time, from Table 7, in the same conditions characterizing the blade, the increase of the pretwist angle exerts an opposite effect to that

Table 7
Effects of the pretwist angle on natural frequencies ω_i (rad/s) of a non-rotating unshearable blade ($\gamma = 0$, $\bar{R}_0 = 0$)

ω_i	Untwisted blade ($\beta_0 = 0$)			Pretwisted blade ($\beta_0 = 40$ deg.)		
	Exact Rosen et al. (1987)	Rosen et al. (1987)	Present	Rosen et al. (1987)	Banerjee (2001)	Present
$i = 1$	3.45305	3.44898	3.45317	3.47257	3.47173	3.47182
$i = 2$	15.4425	15.4184	15.4429	13.2740	13.3465	13.3413
$i = 3$	21.6399	21.5542	21.6406	25.2700	25.1707	25.1677
$i = 4$	60.5924	60.984	60.6120	56.3009	56.3716	56.3485
$i = 5$	96.7764	96.3913	96.7791	103.200	103.263	103.4122

Table 8
Influence of presetting angle on natural frequencies ω_i (rad/s) of a rotating unshearable blade with zero pretwist ($\beta = 0$, $\Omega = 300$ rpm)

ω_i	$\gamma = 0$ deg.		$\gamma = 22.5$ deg.	
	Rosen et al. (1987)	Present	Rosen et al. (1987)	Present
$i = 1$	19.711	19.7183	18.536	18.0769
$i = 2$	32.488	32.4997	33.168	33.4381
$i = 3$	81.585	81.7388	80.620	80.7609
$i = 4$	121.33	121.531	121.97	122.183
$i = 5$	141.62	142.132	141.11	141.618

experienced by the increase of the setting angle. In this sense, as it clearly appears, the increase of the pretwist angle is accompanied, depending on the mode number, i.e. odd or even, by an increase or decrease of the natural frequency, respectively.

7. Numerical simulations and discussion

Although the obtained equations are valid for a beam of arbitrary closed cross-section, for the sake of illustration the case of a rotating beam modelled as a composite box beam (see Fig. 1) characterized by a cross-section ratio $\mathscr{R}(\equiv c/b) = 5$ was considered. In addition, unless otherwise specified, its dimensions are: $L = 80$ in. (2.023 m); $c = 10$ in. (0.254 m); $b = 2$ in. (50.8×10^{-3} m); $h = 0.4$ in. (10.16×10^{-3} m). The mechanical characteristics of the beam as considered in the numerical simulations correspond to the graphite/epoxy material. In the on-axis configuration these are given by

$$E_L = 30 \times 10^6 \text{ psi } (20.68 \times 10^{10} \text{ N/m}^2), \quad E_T = 0.75 \times 10^6 \text{ psi } (5.17 \times 10^9 \text{ N/m}^2)$$

$$G_{LT} = 0.37 \times 10^6 \text{ psi } (2.55 \times 10^9 \text{ N/m}^2), \quad G_{TT} = 0.45 \times 10^6 \text{ psi } (3.10 \times 10^9 \text{ N/m}^2)$$

$$\mu_{TT} = \mu_{LT} = 0.25; \quad \rho = 14.3 \times 10^{-5} \text{ lbs/in}^4 (1528.15 \text{ kg/m}^3)$$

where subscripts L and T denote directions parallel and transverse to the fiber, respectively.

Figs. 2 and 3 display the variation of the first two natural frequencies of the rotating beam ($\Omega = 100$) rad/s, as a function of the ply-angle, for selected values of the setting angle, and for the pretwist, $\beta_0 = 90$ deg.

The results reveal a continuous increase of natural frequencies that accompanies the increase of the ply-angle, Moreover, consistent with the results displayed in Table 7, depending on the odd or even mode number, the increase of the presetting angle yields either a decrease or increase of natural frequencies.

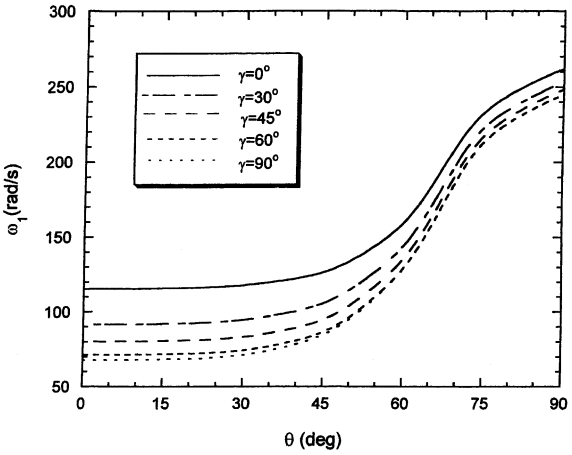

Fig. 2. Variation of the first coupled flapping-lagging natural frequency vs. ply-angle for different setting angles ($\beta_0 = 90$ deg., $\Omega = 100$ rad/s, $\bar{R}_0 = 0.1$).

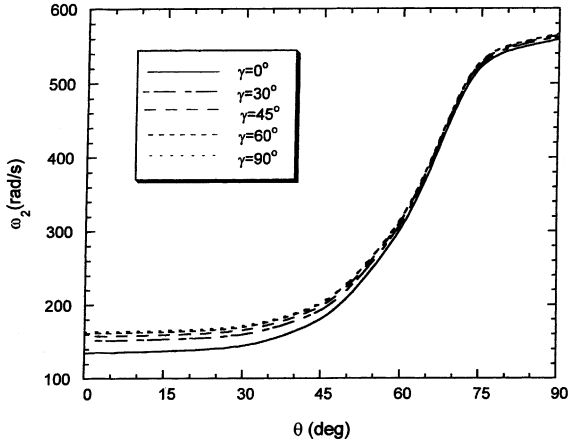

Fig. 3. Variation of the second coupled flapping-lagging natural frequency vs. ply-angle for different setting angles. ($\beta_0 = 90$ deg., $\Omega = 100$ rad/s, $\bar{R}_0 = 0.1$).

Related to these results, one should remark from Figs. 4 and 5 that the increase of the rotational speed yields an increase of natural frequencies as compared to those displayed in Figs. 2 and 3, where a lower angular speed was considered. Moreover, at larger angular speeds, the effect of the ply-angle is more individualized for each of the considered setting angles than in the case of lower angular speeds.

In Figs. 6–8, there is displayed in succession the variation of the first three natural frequencies, as a function of the setting angle, for selected values of the rotational speed. As it clearly appears also from these figures, the effect of the setting angle on eigenfrequency of non-rotating beam is immaterial.

On the other hand, the trend of variation of various mode frequencies as a function of the presetting angle and angular velocity remains similar to that previously emphasized. In these numerical simulations the considered pretwist angle was $\beta_0 = 30$ deg.

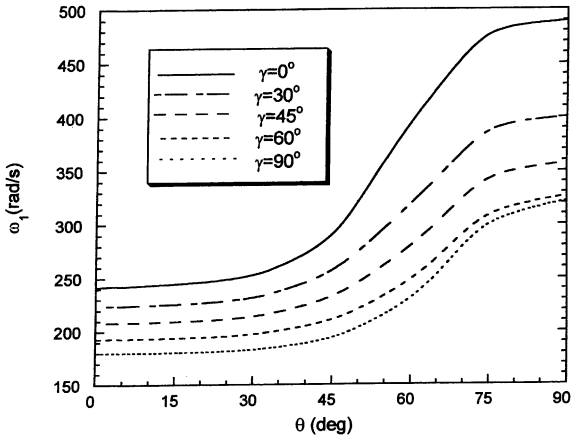

Fig. 4. The counterpart of Fig. 2 for $\Omega = 400$ rad/s.

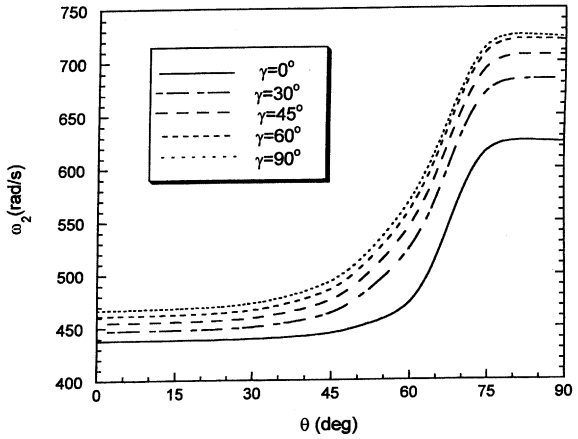

Fig. 5. The counterpart of Fig. 3 for $\Omega = 400$ rad/s.

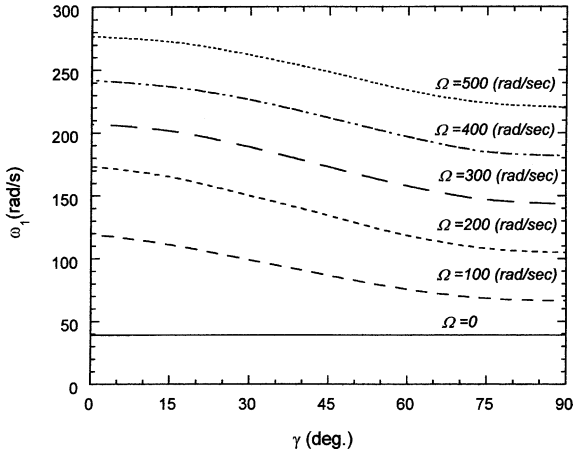

Fig. 6. First coupled flapping-lagging natural frequency vs. presetting angle for selected rotational speeds ($\theta = 0$, $\beta_0 = 30$, $\bar{R}_0 = 0.1$).

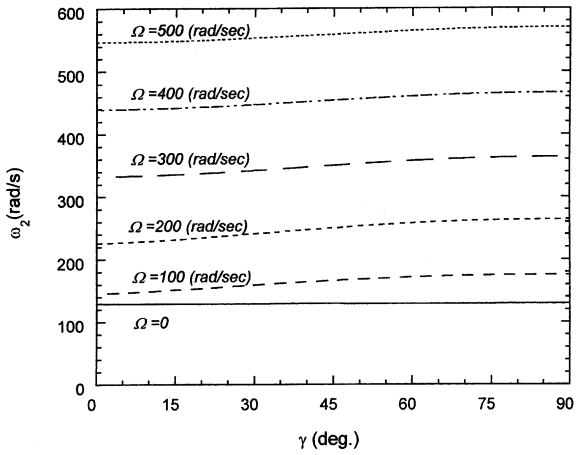

Fig. 7. Second coupled frequency vs. presetting angle for selected rotational speeds ($\theta = 0$, $\beta_0 = 30$ deg., $\bar{R}_0 = 0.1$).

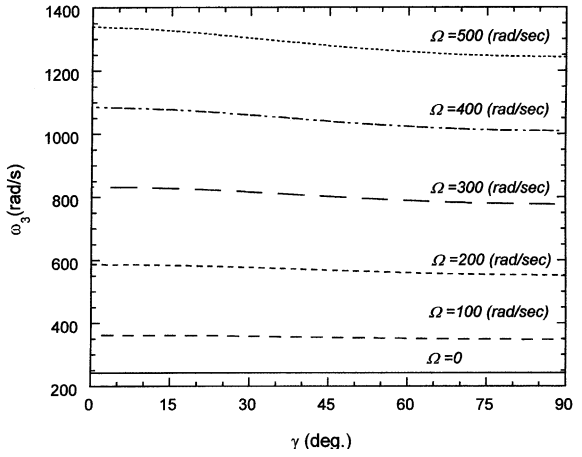

Fig. 8. Third coupled flapping-lagging natural frequency vs. presetting angle for selected rotational speeds ($\theta = 0$, $\beta_0 = 30$ deg., $\bar{R}_0 = 0.1$).

In Figs. 9 and 10, for selected values of the setting angle it is displayed in succession the variation of the first two natural frequencies, as a function of the pretwist angle. For zero presetting angle, the trend of variation of natural frequencies with that of the pretwist angle, coincides with that reported e.g. in the paper by Song et al. (2001a,b). As concerns the frequency variation with that of the setting angle, this is consistent with the trend already indicated in the paper and with that supplied in Table 7.

In Figs. 11 and 12 there are displayed the implications of the hub radius, coupled with that of the rotating speed on the fundamental coupled flapping-lagging natural frequency, for the beam featuring, the setting angles $\gamma = 0$ and 90 deg., and for the ply-angles, in succession, $\theta = 0$ and 45 deg., respectively. Due to the fact that in both cases, as considered in Figs. 11 and 12, the pretwist is $\beta_0 = 90$ deg., the flapping-lagging coupling is present also in the cases involving $\gamma = 0$ and $\theta = 0$.

The results reveal that the differences between the frequencies corresponding to $\gamma = 0$ and 90 deg. tend to decay with the increase of the hub radius. This trend is consistent with that reported in the paper by Kumar

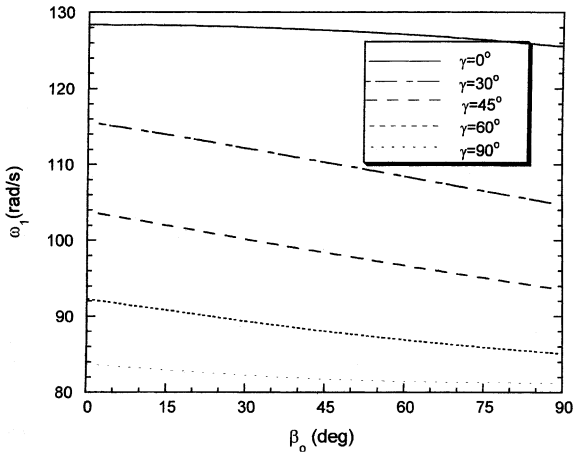

Fig. 9. Variation of the first coupled flapping-lagging natural frequency vs. pretwist angle for different setting angles of the rotating beam ($\theta = 45$ deg., $\Omega = 100$ rad/s, $\bar{R}_0 = 0.1$).

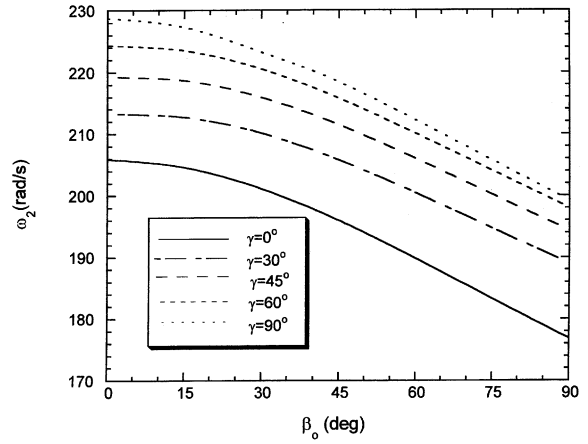

Fig. 10. Variation of the second coupled natural frequency vs. pretwist angle for different setting angles of the rotating beam ($\theta = 45$ deg., $\Omega = 100$ rad/s, $\bar{R}_0 = 0.1$).

(1974). At the same time, the results associated to the same R_0 reveal that the increase of the ply-angle tends to exacerbate the difference between the frequencies corresponding to $\gamma = 0$ and 90 deg.

Figs. 13–15 further emphasize the considerable role that the tailoring technique can play toward the increase, without weight penalties, of the coupled flapping-lagging natural frequencies of rotating beams. Such a role that renders the composite material systems overwhelmingly superior to the metallic structures, deserves well to be highlighted again in these graphs.

In addition, these plots reveal a number of trends related to the implications of the setting angle on each mode frequency, trends that have already been outlined in the previously displayed numerical simulations.

Finally, in Figs. 16 and 17, the first lagging and first flapping normalized mode shapes, respectively, for selected values of the setting angle or of the rotating speed, are supplied. From these plots, it clearly appears that, the flapping mode is much stronger affected by the setting angle/rotating speed, than the lagging mode.

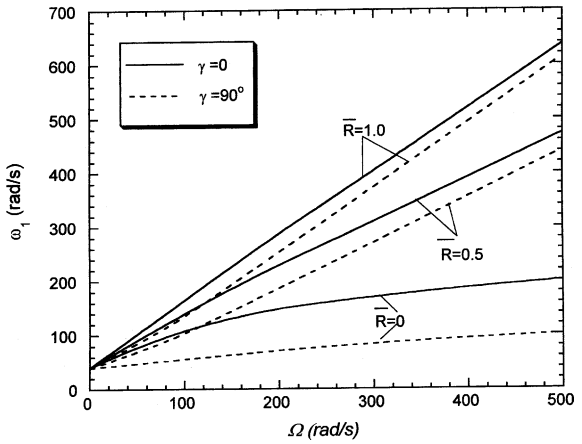

Fig. 11. Variation of the first coupled flapping-lagging natural frequency vs. the rotational speed for different hub radii and two setting angles ($\beta_0 = 90$ deg., $\theta = 0$).

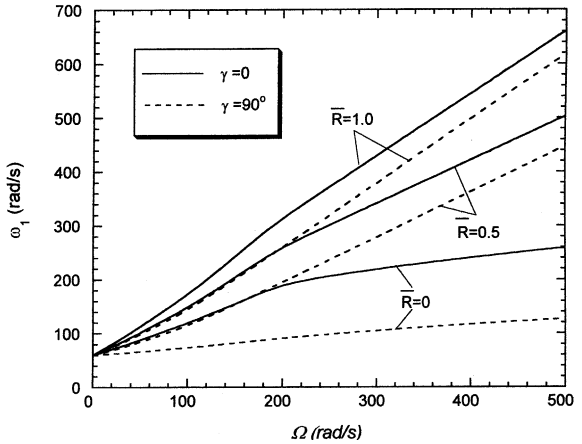

Fig. 12. The counterpart of Fig. 11 for the ply-angle $\theta = 45$ deg.

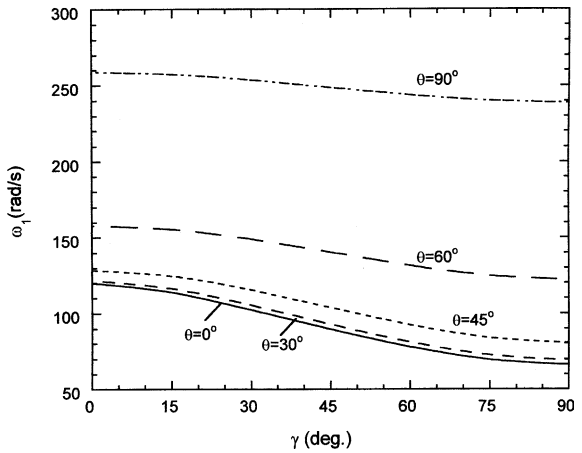

Fig. 13. First coupled flapping-lagging for selected ply-angles ($\beta = 0$, $\Omega = 100$ rad/s, $\bar{R}_0 = 0.1$).

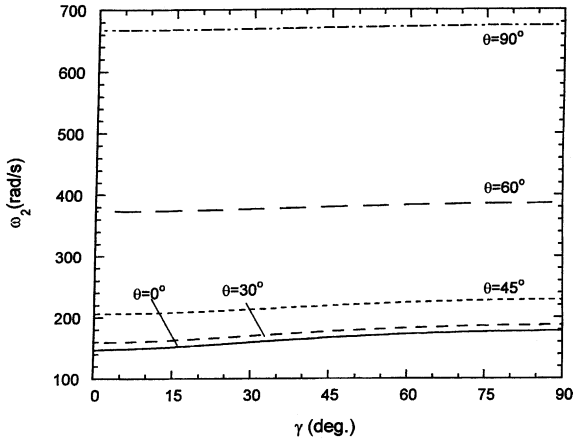

Fig. 14. Second coupled flapping-lagging natural frequency vs. presetting angle for selected ply-angles ($\beta = 0$, $\Omega = 100$ rad/s, $\bar{R}_0 = 0.1$).

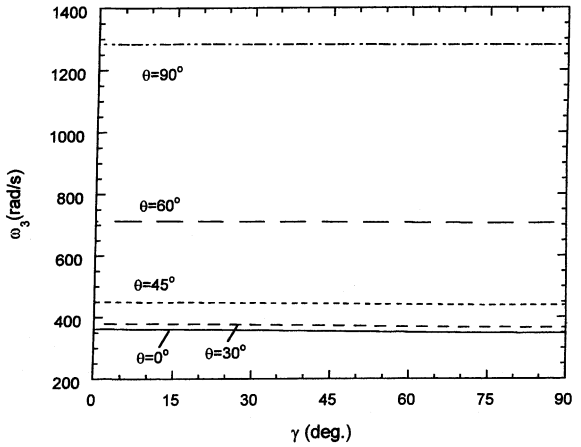

Fig. 15. Third coupled flapping-lagging natural frequency vs. presetting angle for selected ply-angles ($\beta = 0$, $\Omega = 100$ rad/s, $\bar{R}_0 = 0.1$).

8. Conclusions

A dynamic structural model of rotating TWBs encompassing a number of non-classical effects was presented. The developed structural beam model accounts for the effects of the directionality of the fibrous composite materials, and of the elastic couplings induced thereof, transverse shear, rotatory inertias, and of the hub radius. In addition, the effects played by the pretwist and presetting angles, coupled with the previously mentioned ones have been incorporated and their implications on free vibration have been revealed.

Comparisons of eigenfrequency predictions based on the developed model and the extended Galerkin solution methodology used in this paper with some available theoretical and experimental ones for rotating and non-rotating beams have been carried out, and excellent agreements have been reached.

It is hoped that the results reported here will be helpful toward a better understanding of the implications of a number of non-classical effects on natural frequencies of advanced rotating beams, and toward the

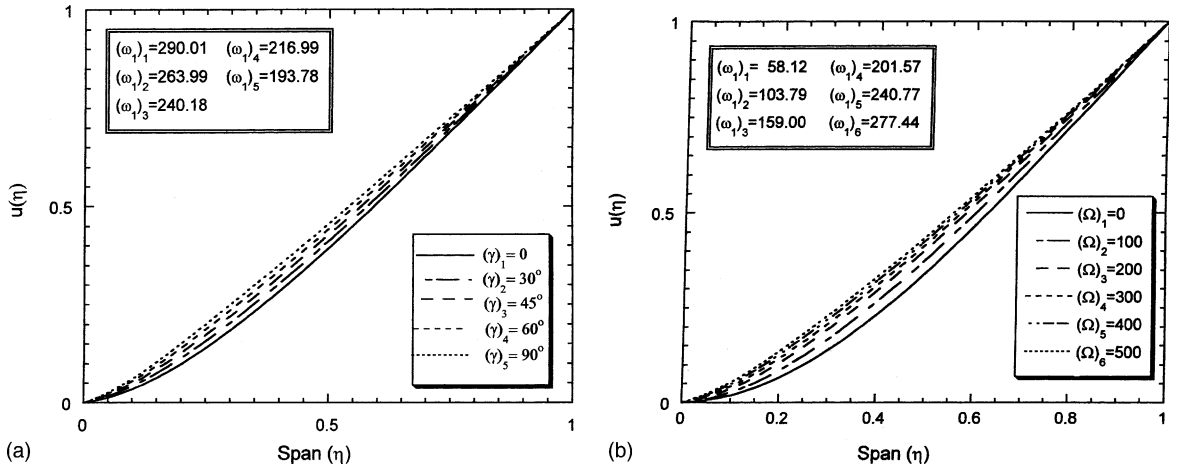

Fig. 16. (a) Variation of the first lagging mode shape in the coupled flapping-lagging for various setting angles ($\beta = 0$, $\Omega = 400$ rad/s, $\theta = 45$ deg., $\bar{R}_0 = 0.1$). The coupled natural frequencies $(\omega_1)_i$ (rad/s) associated with the setting angles are indicated in the inset. (b) Variation of the first lagging mode shape in coupled flapping-lagging for various rotational speeds $(\Omega)_i$ (rad/s) ($\beta = 0$, $\gamma = 45$ deg., $\theta = 45$ deg., $\bar{R}_0 = 0.1$). The coupled natural frequencies $(\omega_1)_i$ (rad/s) associated with the rotational speeds $(\Omega)_i$ (rad/s) are indicated in the inset.

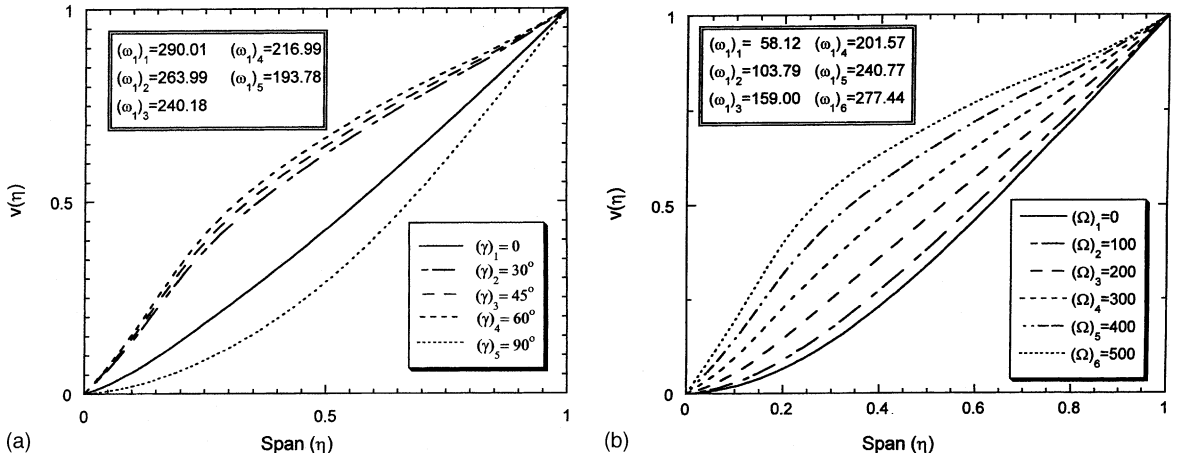

Fig. 17. (a) Counterpart of Fig. 16a for the first flapping mode shape in coupled flapping-lagging motion. (b) Counterpart of Fig. 16b for the first flapping mode shape in coupled flapping-lagging motion.

validation of the finite element and of other approximate methods that are used in the context of the dynamics of rotating beams.

References

Atilgan, A.R., Rehfield, L.W., 1989. Vibration of composite thin-walled beams with designed-in elastic couplings. In: Kobayashi, A. (Ed.), Achievements in Composites in Japan and United States. Fifth Japan–US Conference on Composite Materials, 24–27 June, Tokyo, Japan, pp. 687–694.

Banerjee, J.R., 2001. Free vibration analysis of a twisted beam using the dynamic stiffness method. International Journal of Solids Structures 38, 6703–6722.

Carnegie, W., 1959. Vibrations of pre-twisted cantilever blading. Proc. Inst. Mech. Engrs. London 173, 343.

Carnegie, W., Thomas, J., 1972. The effects of shear deformation and rotary inertia on the lateral frequencies of cantilever beams in bending. Journal of Engineering for Industry, Trans. ASME (February), 267–278.

Chandra, R., Chopra, I., 1992. Experimental-theoretical investigation of the vibration characteristics of rotating composite box beams. Journal of Aircraft 29 (3), 657–664.

Dawson, B., 1968. Coupled bending vibrations of pretwisted cantilever blading treated by Rayleigh–Ritz method. Journal of Mechanical Engineering Science 10, 381.

Hodges, D.H., 1981. An approximation formula for the fundamental frequency of a uniform rotating beam clamped off the axis of rotation. Journal of Sound and Vibration 77, 11–18.

Hodges, D.H., Rutkowski, M.J., 1981. Free-vibration analysis of rotating beams by a variable-order finite element method. AIAA Journal 19, 1459–1466.

Hodges, D.H., 1990. Review of composite rotor blade modeling. AIAA Journal 28, 561–565.

Jung, S.N., Nagaraj, V.T., Chopra, I., 1999. Assessment of composite rotor blade: modeling techniques. Journal of the American Helicopter Society 44 (3), 188–205.

Jung, S.N., Nagaraj, V.T., Chopra, I., 2001. Refined structural dynamics model for composite rotor blades. AIAA Journal 39 (2), 339–348.

Kumar, R., 1974. Vibration of space booms under centrifugal force field. Canadian Aeronautics and Space Institute (CASI) Trans. 7, 1–5.

Kunz, D.L., 1994. Survey and comparison of engineering beam theories for helicopter rotor blades. Journal of Aircraft 31 (3), 473–479.

Lee, S.Y., Lin, S.M., 1996. Bending vibration of rotating nonuniform timoshenko beams with an elastically restrained root. Journal of Applied Mechanics, Trans. ASME, Paper no. 94-WA/ARM-8.

Librescu, L., 1975. Elastostatics and Kinetics of Anisotropic and Heterogeneous Shell-type Structures. Noordhoff International Publishing, Leyden, Netherlands, 560–598.

Librescu, L., Meirovitch, L., Na, S.S., 1997. Control of cantilevers vibration via structural tailoring and adaptive materials. AIAA Journal 35 (8), 1309–1315.

Lo, H., Renbarger, J.L., 1952. Bending vibrations of a rotating beam. Proceedings of the First US National Congress of Applied Mechanics, New York, NY, 75–79.

Putter, S., Manor, H., 1978. Natural frequencies of radially rotating beams. Journal of Sound and Vibrations 56 (2), 175–185.

Qin, Z., Librescu, L., 2001. Static and dynamic validation of a refined thin-walled composite beam model. AIAA Jounral 39 (12), 2422–2424.

Qin, Z., Librescu, L., 2002. On a shear-deformable theory of anisotropic thin-walled beams: further contribution and validations. Composite Structures 56, 345–358.

Rao, J.S., 1977. Coupled vibrations of turbomachine blades. Shock Vibration Bulletin 47, 107.

Rehfield, L.W., Atilgan, A.R., Hodges, D.H., 1990. Nonclassical behavior of thin-walled composite beams with closed cross sections. Journal of the American Helicopter Society 35 (2), 42–51.

Rosen, A., Loewy, R.G., Mathew, B., 1987. Use of twisted principal coordinates and non-physical coordinates in blade analysis. Vertica 11, 541–572.

Rosen, A., 1991. Structural and dynamic behavior of pretwisted rods and beams. Applied Mechanics Reviews, Part 1 44 (12), 483–515.

Slyper, H.A., 1962. Coupled bending vibration of pretwisted cantilever beams. Journal Mechanical Engineering Sciences 4 (4), 365–379.

Smith, E.C., Chopra, I., 1991. Formulation and evaluation of an analytical model for composite box-beams. Journal of the American Helicopter Society 36 (3), 36–47.

Song, O., Librescu, L., 1993. Free vibration of anisotropic composite thin-walled beams of closed cross-section contour. Journal of Sound and Vibration 167 (1), 129–147.

Song, O., Librescu, L., 1997. Structural modeling and free vibration analysis of rotating composite thin-walled beams. Journal of the American Helicopter Society 42 (4), 358–369.

Song, O., Librescu, L., 1999. Modeling and dynamic behavior of rotating blades carrying a tip mass and incorporating adaptive capabilities. Acta Mechanica 134, 169–197.

Song, O., Librescu, L., Oh, S-Y., 2001a. Vibration of pretwisted adaptive rotating blades modeled as anisotropic thin-walled beams. AIAA Journal 39 (2), 285–295.

Song, O., Librescu, L., Oh, S.-Y., 2001b. Dynamic of pretwisted rotating thin-walled beams operating in a temperature environment. Journal of Thermal Stresses 24 (3), 255–279.

Subrahmanyam, K.B., Kulkarni, S.V., Rao, J.S., 1981. Coupled bending–bending vibrations of pretwisted blading allowing for shear deformation and rotary inertia by the Reissner method. International Journal of Mechancial Sciences 23 (9), 517–530.

Volovoi, V.V., Hodges, D.H., Cesnik, C.E.S., Popescu, B., 2001. Assessment of beam modeling methods for rotor blade applications. Mathematical and Computer Modelling 33 (10–11), 1099–1112.

Wang, J.T.S., Mahrenholtz, O., Böhm, 1976. Extended Galerkin's method for rotating beam vibrations using Legendre polynomials. Solid Mechanics Archives 1, 341–356.

Yokoyama, T., 1988. Free vibration characteristics of rotating Timoshenko beams. International Journal of Mechanical Sciences 30 (10), 743–755.